



Cite this: *React. Chem. Eng.*, 2024, 9, 31

Received 3rd November 2023,  
 Accepted 28th November 2023

DOI: 10.1039/d3re00586k

[rsc.li/reaction-engineering](https://rsc.li/reaction-engineering)

## A low-volume flow electrochemical microreactor for rapid and automated process optimization†

Eduardo Rial-Rodríguez,<sup>ab</sup> Johannes F. Wagner,<sup>ab</sup> Hans-Michael Eggenweiler,<sup>c</sup> Thomas Fuchss,<sup>id</sup> Alena Sommer,<sup>c</sup> C. Oliver Kappe,<sup>id</sup> Jason D. Williams<sup>id</sup>\*<sup>ab</sup> and David Cantillo<sup>id</sup>\*<sup>ab</sup>

Electrochemical reactions under constant current can be completed within very short periods of time in microliter-volume cells, as electrolysis time is proportional to the quantity of material processed. A flexible electrochemical microreactor with 17  $\mu$ L volume has been designed and constructed, which enables reactions to be performed in as little as 7.3 s residence time using standard, commercially available electrodes. By utilizing automation and statistical analysis, the reaction design space was explored for three model reactions in 2–3 hours, consuming only 30–300 mg of material for 42 experiments.

Organic electrochemistry is a continuously-growing field that attracts great interest in both academia and industry.<sup>1</sup> This green synthetic technology allows redox transformations to be performed in a cost-effective and safe manner by using electricity as the driving force instead of stoichiometric amounts of oxidants or reductants.<sup>2</sup> Apart from improving the cost efficiency and sustainability of redox transformations, different parameters such as electrode materials<sup>3</sup> or current density provide synthetic organic chemists with additional versatility to optimize and tune reactions.<sup>4</sup>

Despite these advantages, organic electrochemistry has still not become a common tool in synthetic laboratories. In the past, this was mainly due to a lack of standardized equipment and support for non-expert chemists.<sup>5</sup> In recent years, standardized equipment such as the ElectraSyn 2.0 from IKA has been commercialized,<sup>6</sup> improving the accessibility and reproducibility of electrochemistry. However,

most literature on organic electrosynthesis still uses homemade setups assembled from customized parts.<sup>7</sup>

Flow electrolysis cells present several advantages in comparison to their batch counterparts.<sup>8</sup> They provide improved mass transfer and high electrode surface area to reactor volume ratios, which is a key factor in this kind of heterogeneous process where electron transfer takes place at the surface of the electrodes. Additionally, the narrow distance between the electrodes decreases the cell resistance, thus allowing lower concentrations of supporting electrolyte as well as reduced cell voltage, resulting in lower energy consumption. Importantly, flow electrolysis cells are readily scalable.<sup>9</sup>

One unique aspect of bulk electrochemical reactions is that, according to Faraday's Law of electrolysis, the reaction time is proportional to the amount of a substance processed. This means that microreactors featuring a small internal volume allow transformations to be performed in a few seconds.<sup>10</sup> Thus, operating a flow electrochemical microreactor in single-pass mode,<sup>11</sup> which facilitates rapid generation of reaction data whilst minimizing reagent consumption, may represent an ideal approach for the implementation of automation in the development of electrochemical processes.

High-throughput experimentation (HTE) leverages the principles of automation and miniaturization to perform a large number of experiments.<sup>12</sup> This strategy significantly increases the speed and efficiency of reaction screening and optimization, particularly when combined with statistical analysis of results to build reaction models. By utilizing a high throughput approach with a flow microreactor, reaction conditions can be rapidly evaluated and optimized (Fig. 1).

When compared with standard flow reactors,<sup>13</sup> electrochemical microreactors are relatively complex and specific requirements, such as the capability to install different electrode materials, are usually needed. Numerous commercial and homemade continuous flow electrolysis cells have been reported,<sup>7</sup> often consisting of a stack of

<sup>a</sup> Institute of Chemistry, University of Graz, NAWI Graz, Heinrichstrasse 28, 8010 Graz, Austria. E-mail: david.cantillo@uni-graz.at

<sup>b</sup> Center for Continuous Flow Synthesis and Processing (CCFLOW), Research Center Pharmaceutical Engineering GmbH (RCPE), Inffeldgasse 13, 8010 Graz, Austria. E-mail: jason.williams@rcpe.at

<sup>c</sup> Medicinal Chemistry and Drug Design, Merck Healthcare KGaA, Frankfurter Strasse 250, 64293 Darmstadt, Germany

† Electronic supplementary information (ESI) available. See DOI: <https://doi.org/10.1039/d3re00586k>



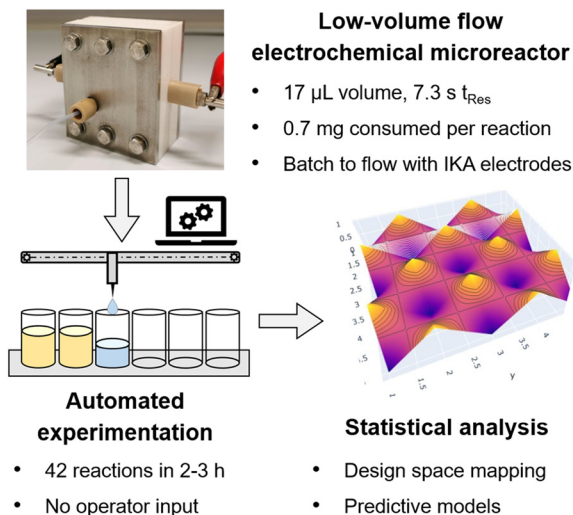


**Fig. 1** Concept for flow electrochemical microreactor, for use in design space scoping, in combination with automation and statistical analysis.

pressed parallel plates (known as a parallel-plate reactor).<sup>14</sup> The reaction mixture is pumped through the gap created between the two electrodes, in either a divided or an undivided cell.

Many laboratory scale flow electrolysis cells designed for single-pass processing are based on “extended channel” designs, which provide longer contact time between the reaction mixture and the surface of the electrode. Reactor volumes ranging from 200  $\mu\text{L}$  and 1000  $\mu\text{L}$  are most common. For example, Willans and coworkers designed a multistep flow platform used to electrochemically generate copper catalysts.<sup>15</sup> Their reactor was built up of circular stacked copper electrodes separated by polytetrafluoroethylene (PTFE) spacers. With a reactor volume of 0.9 mL, each flow electrolysis needed 23 min to reach completion (1.8 h to reach steady state). Commercial cells featuring relatively low volumes include the Flux reactor from Syrris (210  $\mu\text{L}$ )<sup>16</sup> or the Ion reactor from Vapourtec. Wirth and coworkers used the latter (600  $\mu\text{L}$  with a 0.5 mm gap) for the automated synthesis of a library of 54 compounds,<sup>17</sup> although relatively long residence times were employed (6 min). Yoshida developed a microflow cell for organic electrosynthesis,<sup>18</sup> in which several anodic methoxylations were showcased. More recently, Jensen and coworkers utilized an 8  $\mu\text{L}$  reactor for fast screening of a radical-radical cross-coupling.<sup>19</sup> In this case, the flow cell was constructed using a complex micro-fabrication procedure with Pt interdigitated electrodes separated by 10  $\mu\text{m}$  – a design difficult to scale up.

In recent years, standardized batch electrolysis cells such as the IKA ElectraSyn 2.0 have become very popular for small scale batch experimentation. We considered that a flow electrolysis cell that enables implementation of the same electrode dimensions as the batch reactor would significantly improve the transfer from batch to flow, as electrodes used

for batch tests can directly decoupled from the ElectraSyn 2.0 vial and installed in the flow cell.

In this work, we present a novel flow electrochemical microreactor design that utilizes commercially-available batch IKA electrodes (or material from any other supplier cut to the same size). The system therefore is highly versatile in terms of electrode materials, which can be readily exchanged within seconds (Fig. 2). The low cell volume (17  $\mu\text{L}$ ) also enables rapid electrolysis experiments, with residence times as low as 7 s, making the device an ideal tool for automated high-throughput experimentation in flow electrochemistry. The system was validated using three model electrochemical reactions. For each transformation, the electrolysis conditions were optimized in an automated manner. The system showed a high capacity to generate data, with over 40 experiments carried out in *ca.* 2 h, with minimal consumption of chemicals.

The cell consists of two identical PTFE halves, each containing a cavity to fit a commercially-available IKA electrode (Fig. 2, see also Fig. S1–S3 in the ESI†). The reactor channels and interelectrode separator are made of a stack of Mylar foils aligned with the aid of four steel pins. Three 0.1 mm thick layers are used to form the reactor channel, resulting in an interelectrode gap of 0.3 mm. The system is fitted with two steel end plates and 6  $\times$  M6 bolts. Notably, installation of gaskets was generally not necessary to keep the system liquid-tight. However, as the commercially available electrodes from IKA present certain variability in the thickness (2 mm  $\pm$  0.1 mm), PTFE tape was placed between the electrodes and the outer PTFE plate. As the electrode head protrudes from the reactor, the electrical

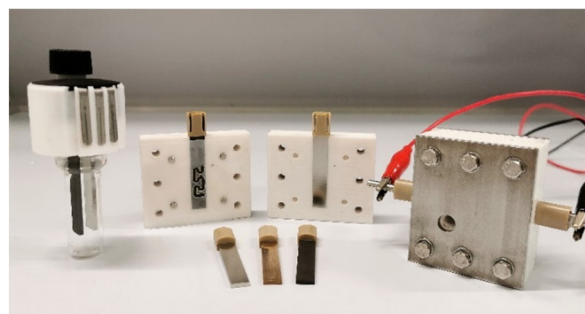
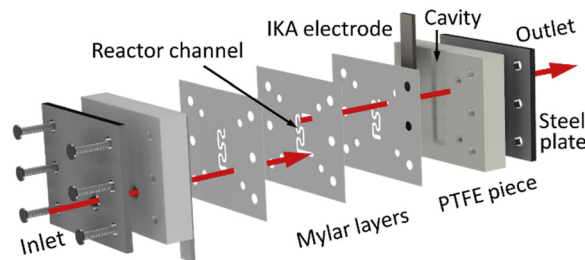


**Fig. 2** Top: Schematic view of the all the layers that form the microreactor: the steel plates, the PTFE pieces and the Mylar layers. Bottom: Photograph of the microreactor closed and open next to the commercial IKA vial for batch electrochemistry.



connection to the power supply can be easily made. The two PTFE halves that form the main body of the cell were manufactured using computer numerical control (CNC) machining, whereas the inner Mylar layers were produced by laser cutting. PTFE and Mylar were chosen as materials for the electrochemical cell due to their excellent chemical resistance and wide availability in machining services.

For each of the 3 model electrochemical reactions evaluated, a set of 42 experiments was performed in a fully-automated manner to study the effect of the current density, amount of charge and flow rate on the reaction yield and productivity. Importantly, the optimal electrode materials were conveniently screened in batch first and then used in the flow reactor. Indeed, the system permitted exactly the

same electrodes to be used in batch and flow mode. The flow microreactor was combined with a syringe pump (Syrris, Asia), a power supply (BK Precision, Model 1739) and a fraction collector (Gilson, GX-241). All devices were controlled using a python script on a single computer (see ESI† for details). At the outlet of the reactor, the reaction mixture was combined with a solvent stream using a T-mixer, diluting the crude reaction mixture stream to a suitable concentration for HPLC analysis. Indeed, the fraction collector placed the diluted aliquots directly in HPLC vials for easy offline analysis.

The first model reaction studied was the 4-electron oxidation of *tert*-butyl toluene (1).<sup>11,20</sup> In this transformation, direct benzylic oxidation of the toluene derivative produces a

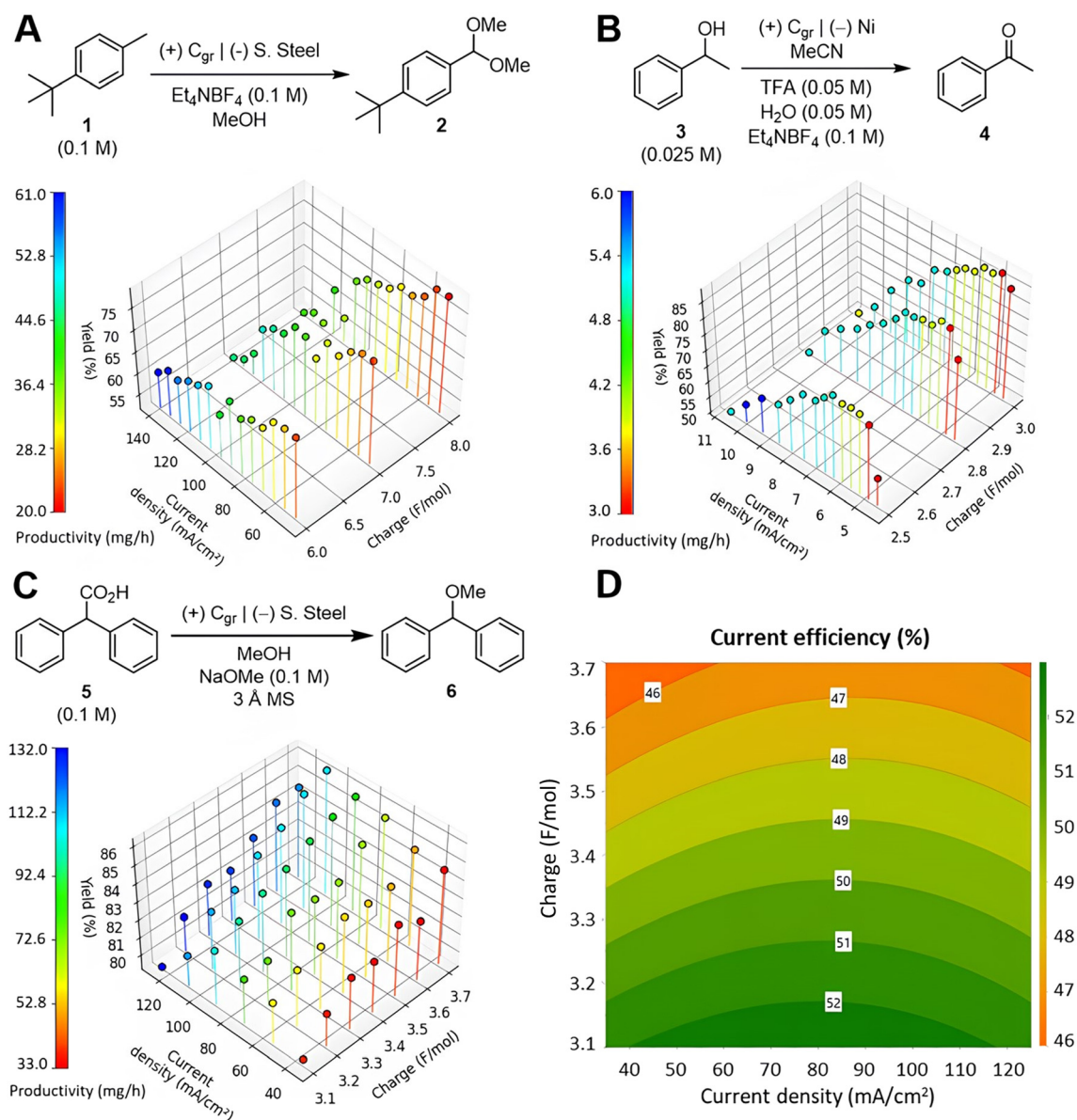


**Fig. 3** Results obtained in the fully-automated runs of three model reactions performed with the microreactor, each with 42 experiments. A) Oxidation of *tert*-butyltoluene 1. B) Oxidation of alcohol 3 to its corresponding ketone. C) Hofer-Moest reaction of carboxylic acid 5. D) Response surface plotted from the model for current efficiency, based on the data collected in C.





carbocation intermediate, which is then rapidly trapped by the reaction solvent, methanol. In the 4-electron process typically observed, the oxidative methoxylation occurs twice, resulting in acetal **2** (Fig. 3A). Under aqueous acidic conditions, **2** is converted into the corresponding aldehyde, which is of industrial interest for the production of crop protection agents among other chemical products.<sup>21</sup>

Due to the small volume of the reactor, only 3.4 mg of substrate per experimental point were consumed during screening. The results showed that the highest yields were achieved with higher charge and lower current density, which led to lower amounts of overoxidation side products. Within each level of charge, the yield steadily decreases as current density increases, until reaching  $\sim 100 \text{ mA cm}^{-2}$ . After this point, a significant decrease in yield can be observed, which is most pronounced when high charge is used. In general, productivity increases with flow rate, aside from in the low-yielding regions at 7 and 8  $\text{F mol}^{-1}$ . Accordingly, the best productivity was achieved with 6  $\text{F mol}^{-1}$  and high charge density (corresponding to high flow rate).

The second example involves the oxidation of a benzylic alcohol to the corresponding ketone.<sup>22</sup> Great efforts have been expended to substitute the traditional heavy metal oxidants with safer and greener options.<sup>23</sup> Due to the abundance of alcohols, their oxidation is usually the way of choice for preparing aldehydes and ketones. In this case, the oxidation of alcohol **3** to acetophenone **4** was chosen as model substrate to illustrate this electrochemical transformation (Fig. 3B).

Since the reaction was carried out with a low substrate concentration (0.025 M), only 0.7 mg of **3** per experiment were consumed. Thus, less than 30 mg of material were required to perform the fully automated set of optimization experiments. In this example, the results show two regions with different trends. In the first one, up to  $6.3 \text{ mA cm}^{-2}$ , yields were generally high with small variations between the experiments. Interestingly, an optimal current density for product formation was identified at  $4.8 \text{ mA cm}^{-2}$ . These results point to a threshold current density (or electrode potential) needed to initiate the anodic oxidation of the alcohol. At higher current densities, the formation of side products was observed, decreasing the selectivity of the reaction and causing a drop in yield. The automated

optimization results led to a maximum productivity value at  $9.3 \text{ mA cm}^{-2}$ , despite not being at the highest flow rate.

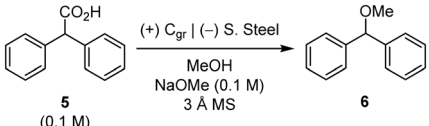
The final example tested was a Hofer–Moest reaction.<sup>24</sup> In this case, a carboxylate is anodically oxidized. Decarboxylation of the ensuing carboxyl radical leads to an alkyl radical, which is further oxidized (in 2-electron process overall) to a carbocation. The cation is trapped by a nucleophile – in the case, the reaction solvent, methanol. The chosen substrate for this reaction was diphenylacetic acid **5**, which readily undergoes the transformation due to the highly stabilized dibenzylic radical formed (Fig. 3C). Since this anodic oxidation is relatively robust, higher current densities and thus higher flow rates were applied compared to previous examples. Therefore, performing the 42 automated experiments only took two hours, 35% faster than the previous two case-studies. Moreover, even though the amount of material employed was slightly higher, only 6.4 mg were consumed per experiment.

The results showed that higher charge led to higher yield, with little influence of the current density. In this case, the superior mass transfer provided by a higher flow rate progressively increased the yield of the reaction until an optimal value was achieved at  $107 \text{ mA cm}^{-2}$ . Beyond that value, a small decrease in yield was observed at the highest current density tested. This is probably due to a decrease in the current efficiency at higher current densities, with energy losses either in the form of heat or generation of side products (*e.g.*, due to solvent oxidation).

Importantly, the large amount of data collected in such a short period enables its processing *via* statistical analysis software. In this case, the software Modde v13 (Sartorius) was used to fit multiple linear regression (MLR) models for yield, productivity and current efficiency outputs. For example, the model for current efficiency (%) for the Hofer–Moest reaction featured an excellent fit ( $R^2 = 0.983$ ,  $Q^2 = 0.975$ ), which facilitates the prediction of results, within the design space covered by the model, using a simple formula. The model can also be conveniently visualized in a surface plot (Fig. 3D).

In general, the model reveals that higher amounts of charge result in lower current efficiency, which is a common trend in electrochemical transformations. As the concentration of substrate **5** decreases, the electrolysis may become mass-transport limited, resulting in lower reaction

**Table 1** Direct scale up of reaction conditions from the microreactor to a larger reactor

					
Entry	Current (mA)	Flow rate ( $\mu\text{L min}^{-1}$ )	Current density ( $\text{mA cm}^{-2}$ )	Charge ( $\text{F mol}^{-1}$ )	Yield (%)
1 <sup>a</sup>	60	113	1.08	3.3	83
2 <sup>b</sup>	689	1300	1.08	3.3	85

<sup>a</sup> Reaction carried out in 17  $\mu\text{L}$  volume microreactor, yield determined by HPLC analysis. <sup>b</sup> Reaction carried out in a larger scale flow reactor ( $6.4 \text{ cm}^2$  electrode surface area, 190  $\mu\text{L}$  volume), isolated yield shown.



rate with concomitant generation of heat or side products. Interestingly, the maximum current efficiency was achieved in a middle range value of current density ( $\sim 80 \text{ mA cm}^{-2}$ ). In this area, mass transfer is improved (due to higher flow rates), yet high electrode potentials (that might oxidize the solvent) are not reached. Full details of all models (9 in total) and statistical analysis can be found in the ESI.† It should be noted that the three model reactions studied herein featured excellent reproducibility and no fouling or degradation of the electrode surface was observed. However, for the study of other reactions it may be advisable to repeat a standard set of conditions periodically to ensure that no decrease in the reaction efficiency occurs.

Finally, to prove that the optimal reaction conditions acquired automatically in the microreactor are scalable, the anodic oxidation of **5** was transferred to a larger flow electrolysis cell featuring the same interelectrode gap (and therefore the same electrode surface area to reactor volume ratio) but an electrode surface area *ca.* 11.5 times larger (Table 1). Gratifyingly, by simply increasing the flow rate and current proportionally to maintain the current density and amount of charge at the optimized value, the reaction proceeded with essentially the same outcome. A slightly higher yield for compound **6** was achieved, probably due to improved mass transfer at higher flow rate. This trend was also observed in the results of the automated run (Fig. 3C).

In conclusion, the design of a 17  $\mu\text{L}$ -volume flow electrochemical microreactor and its combination with automation and statistical analysis has enabled rapid optimization of three reactions. Moreover, because the reactor employs commercial IKA electrodes, it allows efficient transition from batch to flow. The low reactor volume facilitated rapid reactions, with residence times in the range of seconds. Accordingly, very small quantities of material (as low as 0.7 mg) were required for each datapoint in the optimization process. The resulting reaction data could be used to build a range of predictive models to describe reaction performance within the design space. Finally, scalability of the reaction conditions acquired on the small volume electrochemical reactor to a larger flow electrolysis cell (increased electrode surface area by a factor of 11.5) was demonstrated, providing similar results under the same current density and amount of charge. Thus, the automatically generated electrolysis conditions can be used for preparative purposes by simply using a larger reactor with the same interelectrode distance. The developed platform, which can be readily reproduced, may encourage further research in automated flow electrochemistry and expedite electrochemical process development.

## Conflicts of interest

There are no conflicts to declare.

## Acknowledgements

The Research Center Pharmaceutical Engineering (RCPE) is funded within the framework of COMET – Competence Centers for Excellent Technologies by BMK, BMAW, Land Steiermark and SFG. The COMET program is managed by the FFG.

## Notes and references

- (a) A. Wiebe, T. Gieshoff, S. Möhle, E. Rodrigo, M. Zirbes and S. R. Waldvogel, *Angew. Chem., Int. Ed.*, 2018, **57**, 5594–5619; (b) S. R. Waldvogel and B. Janza, *Angew. Chem., Int. Ed.*, 2014, **53**, 7122–7123; (c) M. Yan, Y. Kawamata and P. S. Baran, *Chem. Rev.*, 2017, **117**, 13230–13319; (d) E. J. Horn, B. R. Rosen and P. S. Baran, *ACS Cent. Sci.*, 2016, **2**, 302–308; (e) D. Pollok and S. R. Waldvogel, *Chem. Sci.*, 2020, **11**, 12386–12400; (f) D. S. P. Cardoso, B. Šljukić, D. M. F. Santos and C. A. C. Sequeira, *Org. Process Res. Dev.*, 2017, **21**, 1213–1226; (g) S. Möhle, M. Zirbes, E. Rodrigo, T. Gieshoff, A. Wiebe and S. R. Waldvogel, *Angew. Chem., Int. Ed.*, 2018, **57**, 6018–6041.
- (a) D. Cantillo, *Chem. Commun.*, 2022, **58**, 619–628; (b) B. A. Frontana-Urbe, R. D. Little, J. G. Ibanez, A. Palma and R. Vasquez-Medrano, *Green Chem.*, 2010, **12**, 2099–2119.
- D. M. Heard and A. J. J. Lennox, *Angew. Chem.*, 2020, **59**, 18866–18884.
- C. Kingston, M. D. Palkowitz, Y. Takahira, J. C. Vantourout, B. K. Peters, Y. Kawamata and P. S. Baran, *Acc. Chem. Res.*, 2020, **53**, 72–83.
- (a) S. B. Beil, D. Pollok and S. R. Waldvogel, *Angew. Chem.*, 2021, **60**, 14750–14759; (b) M. Yan, Y. Kawamata and P. S. Baran, *Angew. Chem., Int. Ed.*, 2018, **57**, 4149–4155.
- N. Fu, G. S. Sauer and S. Lin, *Nat. Protoc.*, 2018, **13**, 1725–1743.
- D. Pletcher, R. A. Green and R. C. D. Brown, *Chem. Rev.*, 2018, **118**, 4573–4591.
- (a) T. Noël, Y. Cao and G. Laudadio, *Acc. Chem. Res.*, 2019, **52**, 2858–2869; (b) M. Elsherbini and T. Wirth, *Acc. Chem. Res.*, 2019, **52**, 3287–3296; (c) T. P. Nicholls, C. Schotten and C. E. Willans, *Curr. Opin. Green Sustainable Chem.*, 2020, **26**, 100355; (d) N. Tanbouza, T. Ollevier and K. Lam, *iScience*, 2020, **23**, 101720; (e) M. Atobe, H. Tateno and Y. Matsumura, *Chem. Rev.*, 2018, **118**, 4541–4572; (f) M. A. Bajada, J. Sanjosé-Orduna, G. Di Liberto, S. Tosoni, G. Pacchioni, T. Noël and G. Vilé, *Chem. Soc. Rev.*, 2022, **51**, 3898–3925.
- C. Bottecchia, D. Lehnher, F. Lévesque, M. Reibarkh, Y. Ji, V. L. Rodrigues, H. Wang, Y. H. Lam, T. P. Vickery, B. M. Armstrong, K. A. Mattern, K. Stone, M. K. Wismer, A. N. Singh, E. L. Regalado, K. M. Maloney and N. A. Strotman, *Org. Process Res. Dev.*, 2022, **26**, 2423–2437.
- R. Green, R. Brown and D. Pletcher, *J. Flow Chem.*, 2015, **5**, 31–36.
- S. Maljuric, W. Jud, C. O. Kappe and D. Cantillo, *J. Flow Chem.*, 2020, **10**, 181–190.



- 12 (a) J. Rein, J. R. Annand, M. K. Wismer, J. Fu, J. C. Siu, A. Klapars, N. A. Strotman, D. Kalyani, D. Lehnher and S. Lin, *ACS Cent. Sci.*, 2021, **7**, 1347–1355; (b) M. Shevlin, *ACS Med. Chem. Lett.*, 2017, **8**, 601–607.
- 13 M. B. Plutschack, B. Pieber, K. Gilmore and P. H. Seeberger, *Chem. Rev.*, 2017, **117**, 11796–11893.
- 14 (a) C. Gütz, A. Stenglein and S. R. Waldvogel, *Org. Process Res. Dev.*, 2017, **21**, 771–778; (b) W. Jud, C. O. Kappe and D. Cantillo, *Chem.: Methods*, 2021, **1**, 36–41; (c) B. Gleede, M. Selt, C. Gütz, A. Stenglein and S. R. Waldvogel, *Org. Process Res. Dev.*, 2020, **24**, 1916–1926; (d) H. R. Stephen, S. Boyall, C. Schotten, R. A. Bourne, N. Kapur and C. E. Willans, *React. Chem. Eng.*, 2022, **7**, 264–268.
- 15 C. Schotten, J. Manson, T. W. Chamberlain, R. A. Bourne, B. N. Nguyen, N. Kapur and C. E. Willans, *Catal. Sci. Technol.*, 2022, **12**, 4266–4272.
- 16 R. A. Green, R. C. D. Brown and D. Pletcher, *J. Flow Chem.*, 2015, **5**, 31–36.
- 17 N. Amri and T. With, *Synthesis*, 2020, **52**, 1751–1761.
- 18 R. Horcajada, M. Okajima, S. Suga and J.-I. Yoshida, *Chem. Commun.*, 2005, 1303–1305.
- 19 Y. Mo, G. Rughoobur, A. M. K. Nambiar, K. Zhang and K. F. Jensen, *Angew. Chem., Int. Ed.*, 2020, **59**, 20890–20894.
- 20 (a) G. P. Roth, R. Stalder, T. R. Long, D. R. Sauer and S. W. Djuric, *J. Flow Chem.*, 2013, **3**, 34–40; (b) D. S. P. Cardoso, B. Šljukić, D. M. F. Santos and C. A. C. Sequeira, *Org. Process Res. Dev.*, 2017, **21**, 1213–1226.
- 21 H. J. Schäfer, *C. R. Chim.*, 2011, **14**, 745–765.
- 22 (a) E. A. Mayeda, *J. Am. Chem. Soc.*, 1975, **97**, 4012–4015; (b) E. A. Mayeda, L. L. Miller and J. F. Wolf, *J. Am. Chem. Soc.*, 1972, **94**, 6812–6816; (c) D. Wang, P. Wang, S. Wang, Y. H. Chen, H. Zhang and A. Lei, *Nat. Commun.*, 2019, **10**, 1–8.
- 23 D. J. C. Constable, P. J. Dunn, J. D. Hayler, G. R. Humphrey, J. L. Leazer Jr., R. J. Linderman, K. Lorenz, J. Manley, B. A. Pearlman, A. Wells, A. Zaks and T. Y. Zhang, *Green Chem.*, 2007, **9**, 411–420.
- 24 (a) H.-J. Schäfer, *Top. Curr. Chem.*, 1990, **152**, 91–151; (b) H. Hofer and M. Moest, *Liebigs Ann.*, 1902, **323**, 284–323.

